An observational study of a magneto-acoustic wave in the solar corona

D. R. Williams,[1,2]★ M. Mathioudakis,[1] P. T. Gallagher,[3] K. J. H. Phillips,[4]
R. T. J. McAteer,[1] F. P. Keenan,[1] P. Rudawy[5] and A. C. Katsiyannis[1]

[1]*Department of Pure and Applied Physics, The Queen's University of Belfast, Belfast BT7 1NN*
[2]*Mullard Space Science Laboratory, University College London, Holmbury St Mary, Surrey RH5 6NT*
[3]*L3 Com Analytics Corp., NASA Goddard Space Flight Centre, Greenbelt, MD 20771, USA*
[4]*Space Science & Technology Department, Rutherford Appleton Laboratory Chilton, Didcot, Oxon OX11 0QX*
[5]*Astronomical Institute, University of Wrocław, Wrocław, Poland*

ABSTRACT

The Solar Eclipse Corona Imaging System (SECIS) observed a strong 6-s oscillation in an active region coronal loop, during the 1999 August 11 total solar eclipse. In the present paper we show that this oscillation is associated with a fast-mode magneto-acoustic wave that travels through the loop apex with a velocity of 2100 km s^{-1}. We use near-simultaneous *SOHO* observations to calculate the parameters of the loop and its surroundings such as density, temperature and their spatial variation. We find that the temporal evolution of the intensity is in agreement with the model of an impulsively generated, fast-mode wave.

Key words: MHD – waves – eclipses – Sun: activity – Sun: corona – Sun: oscillations.

1 INTRODUCTION

The debate concerning MHD wave heating of the solar corona tends to centre on the feasibility of Alfvén and magneto-acoustic waves reaching into the corona and damping sufficiently quickly to balance the observed radiative losses. Porter, Klimchuk & Sturrock (1994a,b) have examined the processes of coronal heating by slow- and fast-mode high-frequency MHD waves. They conclude that heating of coronal active regions by slow-mode waves is viable for periods $\tau \lesssim 100$ s and by fast-mode waves with periods $\tau \lesssim 1$ s. Although slow-mode magneto-acoustic waves may contribute significantly to the energy balance of the corona, only the fast-mode waves can damp sufficiently quickly to balance the typical active region radiative loss rates.

In an earlier article (Williams et al. 2001), we presented observations of an oscillation of period 6 s in an active region coronal loop. These observations were performed on the so-called coronal 'green line' of Fe XIV at 5303 Å, with the high-cadence, joint UK–Polish SECIS instrument (Phillips et al. 2000). Periodic modulations in the period range 10–60 s have been previously reported in the active, non-flaring corona (McKenzie & Mullan 1997). The observations we presented, however, are unique as they are taken in visible light at extremely high cadence: SECIS is a twin-CCD, high cadence instrument which takes synchronized image sequences in both white light and the Fe XIV green line. This system is capable of detecting periodic behaviour at frequencies of up to 30 Hz.

The detection of the 6-s oscillation was made in Fe XIV (5303 Å) in a 4×10^4 km portion of the loop apex. The reported detections

were all above the 99 per cent confidence level, using wavelet analysis to isolate the quasi-periodic phase of the wave in time. No corresponding oscillation was seen in the open white light channel of SECIS. The peak-to-peak amplitude of the wave was 5.5 per cent of the unperturbed Fe XIV intensity. This is somewhat larger than the 1–2 per cent variation reported by Pasachoff & Landman (1984) and the 0.2–1.3 per cent amplitude of Singh et al. (1997) in a comparable frequency range, both from analogous experiments.

We have suggested (Williams et al. 2001) that the 6-s oscillation might make a significant contribution to the energy input of the coronal loop, since it has a frequency comparable to the allowable range of Porter et al. (1994b). In the present paper we examine in detail the properties of both the loop and the oscillation observed within.

2 OBSERVATIONS AND DATA ANALYSIS

2.1 SECIS

2.1.1 Observations

Our observations were made on 1999 August 11 during the total solar eclipse in Shabla, Bulgaria, sampling at high cadence (44 frames per second) giving a maximum detectable frequency of 22 Hz. The 35-arcmin field-of-view of the observations included a portion of the Sun from the north-east limb to the west limb, a region which contained two prominent active regions. One active region loop in particular, in NOAA AR 8651, stands out in the Fe XIV data set, and was therefore chosen for analysis. This loop can be seen clearly in an image of Fe XII taken at the same
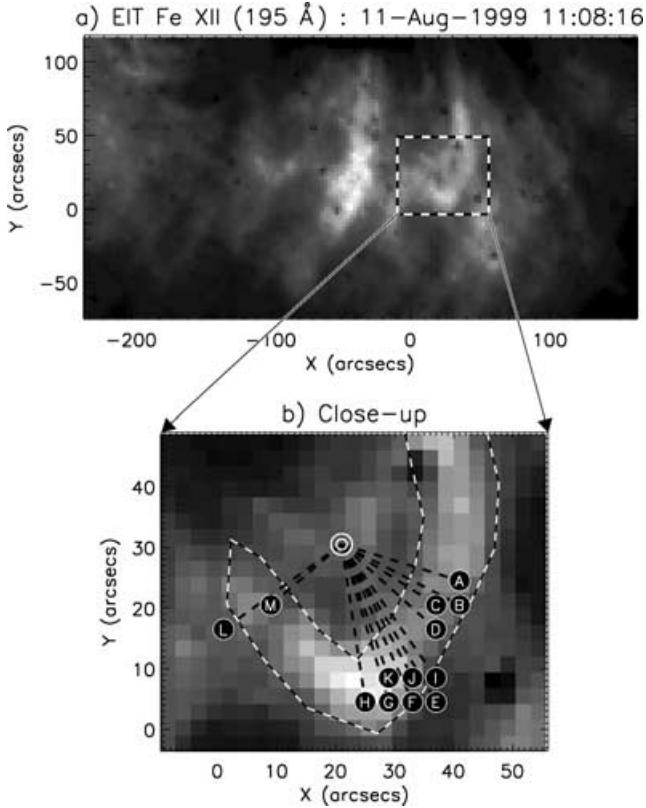
★E-mail: drw@mssl.ucl.ac.uk

Figure 1. (a) Prominent loops in active region NOAA AR 8651, as observed in *SOHO*/EIT Fe XII (195 Å). The EIT field of view has been rotated 123° clockwise in order to directly compare it with SECIS images. The origin given is the origin of the grid of points, around the selected loop, which were examined for periodicity (Fig. 2b); (b) close-up on the chosen loop, showing the indexed points at which SECIS detected the 0.16-Hz oscillation. Radials from an approximate centre-of-curvature for the loop apex (indicated by a double white circle) are shown. The angles made by these radials to the horizontal are used to express an *angular* position for each index along the apex. This figure is available in colour on *Synergy*, the electronic version of the journal.

time as the eclipse by the EUV Imaging Telescope (EIT; Fig. 1) of the *Solar and Heliospheric Observatory* (*SOHO*). The plasma temperature sampled ($\log T_{\text{Fe XII}} = 6.15$) is similar to that observed at 5303 Å ($\log T_{\text{Fe XIV}} = 6.25$).

The 6-s periodicity was found in thirteen different positions in a grid of pixels around this coronal loop in the SECIS Fe XIV sequence. The time-averaged Fe XIV image is shown in Fig. 2. To enhance the signal-to-noise ratio in the data set, the intensity shown at each pixel is in fact the intensity due to that pixel and the eight adjacent pixels; i.e. we sum over a 3×3 pixel^2 area. The scale of the pixels shown is 4.07 arcsec and each point which exhibits this periodic intensity fluctuation is denoted by an alphabetical index **A–M**. As can be seen, each of these indexed points corresponds to a point on this loop in active region AR 8651.

Because of errors in the pointing introduced into the data by a mechanism beyond the control of the observing team, only the first 40 s of the 144-s data sequence was free from contamination by false oscillations. These false peaks in Fourier space were identified by both wavelet analysis (Williams et al. 2001) and discrete Fourier analysis (Rudawy et al. 2001). In neither case was an oscillation found to be introduced at (or near) 0.16 Hz. Detections at this frequency are therefore presumed to be solar in origin.
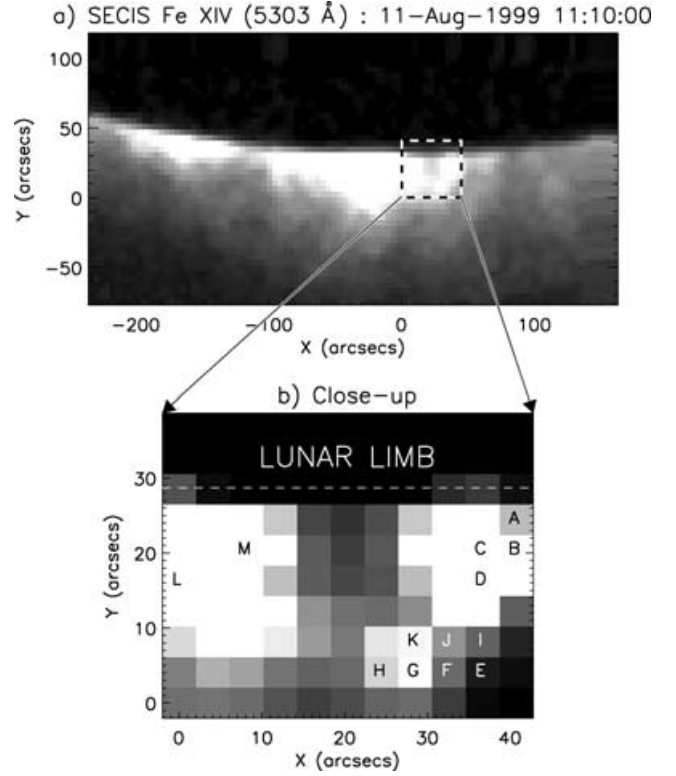

Figure 2. (a) A SECIS time-averaged Fe XIV 5303 Å image. The image is an average over 50 consecutive frames (1.1 s) from the beginning of the sequence, and has been contrast-enhanced to better demonstrate the presence of the active region loop chosen for analysis; (b) region of image around the active region loop. The image has been contrast-enhanced. This figure is available in colour on *Synergy*, the electronic version of the journal.

In our earlier paper, we interpreted the spatial correlation between the loop and the points that exhibited the 6-s periodic fluctuations as evidence that the oscillation was unique to this loop. This oscillation was not found in points (in the focal plane) spatially removed from the loop, including those of high signal in and around the core of the active region.

2.1.2 Evidence of a travelling wave

A detailed investigation of the light curves of individual points along the loop strongly indicates that the maxima and minima of this oscillation are a function of both position and time. Plotting the intensity at each point as a function of time, the maximum of the intensity of the wave is shown to move along the apex of the loop in an anti-clockwise sense. Fig. 3 demonstrates the light curve for each indexed point **A–K**, the curves being ordered by increasing distance around the apex from point **L**. The light curves are smoothed with a running boxcar average of width 1 s, and the extent of the variation in intensity (given in count exposure^{-1}) is delimited by the vertical axis to the left of each curve. It can immediately be noted that the brightest part of the wave occurs at **H** before point **G** and so on, through to point **A**.

In order to assess the nature of this wave, and determine its mode, it is necessary both to gauge its speed, and to estimate the local magnetic field strength, electron temperature and density in both the loop and the ambient plasma.
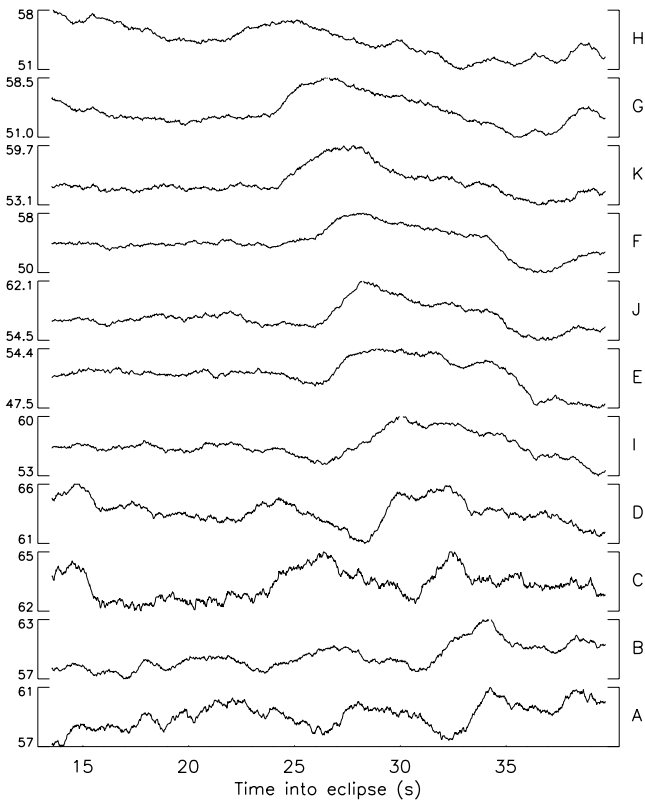
Figure 3. Plot of the intensity, in the SECIS Fe XIV channel, at each alphabetical index point (as per Fig. 2) as a function of time after the beginning of the eclipse. Each light curve has been smoothed with a running boxcar average of width 1 s. The vertical range on each light curve denotes the intensity range of the light curve, in counts per exposure. The amplitude of the wave is determined from the peak-to-peak variation in the oscillatory portion of the light curve and is found to be 5.5 per cent. The light curves are plotted sequentially according to increasing distance from point **L** along the loop apex. This demonstrates the motion of the peak intensity, whose progress is more quantitatively charted in Fig. 6.

2.2 SOHO observations and analysis

We use observations obtained with the Coronal Diagnostic Spectrometer (CDS) on *SOHO* in its normal incidence mode (the Normal Incidence Spectrograph, NIS), to determine both the temperature and density for AR 8651, where the selected loop was found. These observations were requested as support data for SECIS and were carried out on the day of the eclipse. As stated in our previous article, the loop we examine is partially obscured by a prominence and neighbouring loops, to the extent that only the northern leg of the loop is observable to us.

To examine the local plasma conditions, we use two NIS rasters which overlap spatially in the region of the loop (Fig. 4). The 'lower' raster is centred on heliocentric co-ordinates (900″, 500″) and was taken at ∼17:00 UT, while the 'upper' raster, taken at ∼18:00 UT, was centred on (800″, 650″). We use the temperature-sensitive, but density-insensitive, line ratio of Fe XIV (334.2 Å)/Fe XIII (348.2 Å) (Brosius et al. 1994) to determine a temperature within the loop of 2.5×10^6 K, with little variation ($\approx 2.5 \times 10^5$ K) along its observable length. We also deduce the temperature along a comparable (heliocentric) radial distance outside the loop, but within the same active region. The temperature along this radial is found to be almost identical (Fig. 5). We have also used EIT data to infer the temperature of the plasma. Using the filter ratio technique of Zhang, White
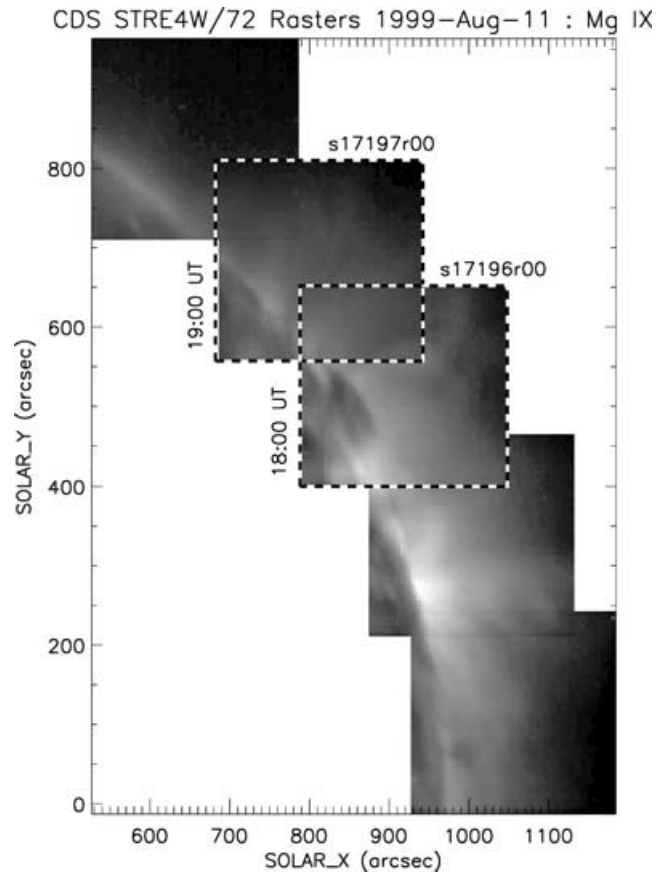

Figure 4. Mosaic of several STRE4W72 CDS rasters taken in the vicinity of the field of view of SECIS on 1999 August 11, with the two rasters analysed outlined by a dashed line. The images shown are in the 398 Å line of Mg IX. The 'lower' (i.e. southern) raster is the earlier of the two, and was taken between 17:16 and 18:31 UT. The 'upper' raster was made between 18:32 and 19:47 UT. Approximate times are shown to the left of each raster.
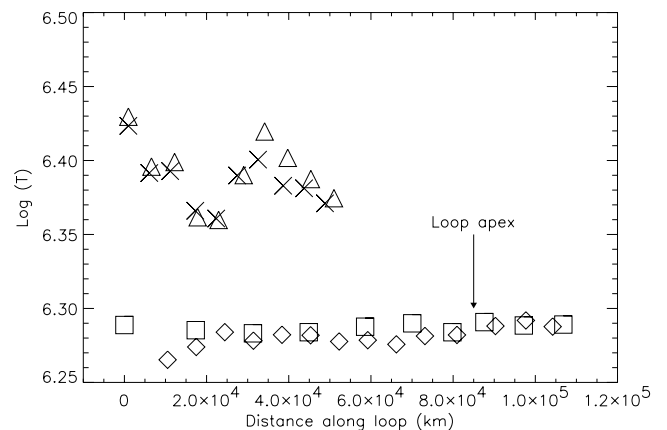

Figure 5. Temperature of the loop determined from CDS and EIT data taken on 1999 August 11. The squares represent the temperature along the loop, and diamonds the temperature outside the loop, as calculated from EIT filter ratios, an hour after eclipse. The triangles denote temperatures within the loop derived from CDS measurements of the Fe XIV/Fe XIII ratio, while crosses represent the temperature calculated outside the loop along a parallel path. A small systematic difference in the values of temperature between the two methods is due to the different ions and techniques involved.

& Kundu (1999), we have constructed full-disc temperature maps of the Sun at 12:20 UT. By taking a profile along the loop – relatively unchanged since the time of eclipse – we have found a temperature of $T \sim 2 \times 10^6$ K both inside and outside the loop (Fig. 5), only slightly different from the value obtained using CDS line ratios.

To infer the local density, we use the density-sensitive line ratio of Fe XIV 334.2 Å/353.8 Å in the CHIANTI data base (Dere et al. 1997), which samples the same plasma temperature as the green line. Using this method, we find an electron density of $N_e = 2 \times 10^9$ cm^{-3} within the loop, and an external electron density of $N_{e\,\mathrm{ext}} = 8 \times 10^8$ cm^{-3}.

Given the time difference between the SECIS and NIS observations, it is important to remember that the derived plasma values can only be used as an indication for the actual conditions during the eclipse (11:10 UT). However, we believe that, given the diversity of active regions and the prevalence of 'typical coronal values' in the literature, our approach provides an accurate way for estimating the local conditions which may in turn be used to identify the physical processes within the loop.

3 DESCRIPTION OF THE WAVE

3.1 Wave velocity

In a low-β plasma ($\beta \ll 1$), of which the corona is an example, a wave travelling at a velocity of the order of the local sound speed c_s (typically ~ 200 km s^{-1}) can usually be classified as a slow-mode magneto-acoustic wave. Similarly, a wave travelling at a speed tending to the local Alfvén velocity v_A (typically ~ 2000 km s^{-1}), will normally be a fast-mode wave.

We use the following procedure to estimate the group velocity of the wave, v_g – the speed at which the wave actually transports energy. The outline of the loop is determined from EIT Fe XII λ195 images and shown in Fig. 1(b). Plotted over the dotted loop outline are the oscillation's position indices. Lastly, radials (black dashed lines) are drawn from each index to an approximate centre-of-curvature (white circles). The angle made by each line to the radial drawn by point **L** can be taken and assigned to each index as its *angular* position; point **L** is chosen as the origin as it is the furthest point clockwise along the loop in Fig. 1.

An average radius, from the centre-of-curvature, is necessary to deduce each point's distance along the loop from point **L**. Since we are concentrating on points **A** to **K**, we take the average length of only these points' radials, which gives a value of 1.8×10^9 cm (25 arcsec). Using this radius of curvature, we find each point's distance along the loop from **L**. The time of arrival of the wave's maximum intensity, $t_{\max}$ is defined as the time – during the interval $20\,\mathrm{s} < t < 40\,\mathrm{s}$ – when the maximum intensity is reached. Plotting each point's distance along the loop against $t_{\max}$ produces a straight line whose gradient gives the group velocity v_g, of the wave. This plot is shown in Fig. 6, indicating a group velocity of approximately 2.1×10^8 cm s^{-1} (2100 km s^{-1}). If we assume that the phase velocity $v_{\mathrm{ph}} \approx v_g$, then we can calculate a wavelength of 1.2×10^9 cm. The derived value for the velocity is very similar to canonical values for the coronal Alfvén velocity v_A, which leads us to conclude that this wave is fast-mode.

3.2 Wavelength and phase

An additional piece of evidence for the wave's travelling nature is gleaned from the discrete Fourier transform of the 40-s time se-
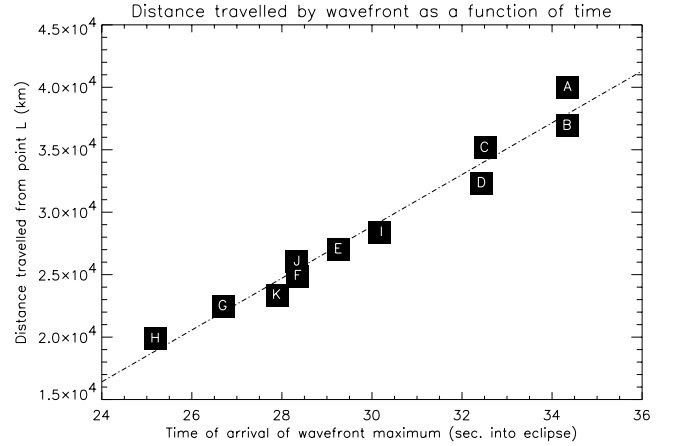

Figure 6. Plot of distance travelled by wave maximum along loop from point **L** as a function of time after the beginning of totality. The line of best fit through these points is the effective speed of the wave through the loop apex.
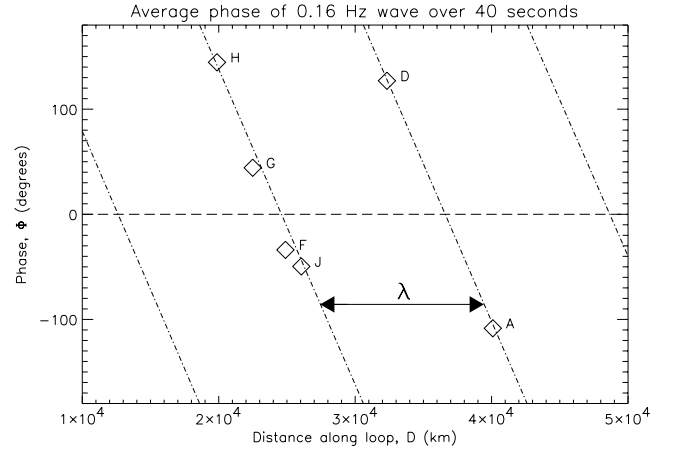

Figure 7. Plot of time-averaged wave phase Φ as a function of distance along the loop. The phase is calculated from the real and imaginary parts of the fast Fourier transform (FFT), which in turn is computed from the entire 40-s time series available. The separation of the dot–dashed lines gives the wavelength λ of the wave.

ries at the various points along the loop. Fig. 7 shows the time-averaged phase of the wave at the each position index. It must be stated that these phases are averaged over the 40 s of the input time series. As such, they represent a time-averaged snapshot of the wave along the loop. Since phase, Φ, has a wrap-around effect at $\Phi = 180° = -180°$, parallel lines can be drawn through the values of Φ as a function of distance along the loop, D. The period (in D) is therefore equal to the wavelength of a travelling wave, and is again found to be $\lambda = 1.2 \times 10^9$ cm. We can therefore say that the phase and group velocities of the wave are, to a very good approximation, equal.

4 RESULTS AND DISCUSSION

Roberts, Edwin & Benz (1984) discuss the properties and evolution of fast and slow magneto-acoustic waves, both standing and impulsively generated. In this context, consider Fig. 8 which shows the wavelet transform of a time series formed from the intensity at point **A** in Fig. 2. It can be seen that during the first half of this
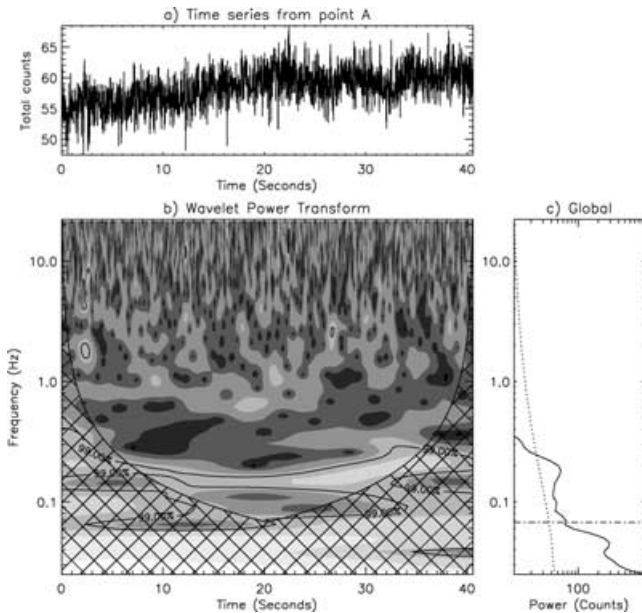
Figure 8. (a) The light-curve recorded at point **A** in Fig. 2; (b) wavelet power transform of this light-curve; (c) global wavelet power spectrum, analogous to a Fourier power spectrum. The frequency of 0.16-Hz (6-s period) is clearly visible (panel b) in the second half of the time series. This figure is available in colour on *Synergy*, the electronic version of the journal.

40-s time series, the 0.16-Hz frequency oscillation is not detected. Roberts et al. (1984) detail the evolution of an impulsively generated fast wave as: (i) an initial periodic phase, beginning at a time $\propto 1/v_{Ae}$ after the initial impulse (where v_{Ae} is the external Alfvén velocity $= B/\sqrt{4\pi m_p N_{e\,ext}}$), characterized by an increase in amplitude and an accompanying gradual increase in frequency; (ii) a quasi-periodic phase, at a time $\propto 1/v_A$, showing a marked increase in amplitude; and (iii) a periodic decay phase with a rapid decrease in amplitude. This result is mirrored in the models of Berghmans, De Bruyne & Goossens (1996), who analyse the progression of an impulsively driven wave along a loop.

Since the wave we observe is characterized by a travelling wavefront and a trailing wake (of negative amplitude), it is of interest to compare the findings of Roberts et al. (1984) with our observations. The onset of the detected 6-s periodicity occurs at a time ~ 20 s after the beginning of eclipse ($t = 0$). Given the time series of our observations, this presents us with two possible interpretations. It may be the case that the wave is observed in its periodic phase, with the information being carried along the loop at v_{Ae}. In this instance, the onset of a detectable oscillatory component may be due to the gradual increase in amplitude to the level where it is detected above the noise. The corresponding increase in frequency, due to the arrival of progressively faster frequency information, arises because of the dispersion relation of the fast-mode wave. Wavelet transforms enjoy only limited frequency resolution, however, and a small increase in frequency may have gone undetected in our data.

Alternatively, the emergence of signal from below the noise level may be due to the onset of the quasi-periodic phase with its associated leap in amplitude. The difficulty in assigning the observed periodicity to either of these scenarios lies in both the limited signal-to-noise ratio of the available SECIS data, and the length of the time series, since the observed periodicity continues until – and perhaps beyond – the end of the time series. Furthermore, both the periodic and quasi-periodic phases of the impulsively generated wave are partially characterized by an increase in amplitude. The power in

the 0.16-Hz band (Fig. 8) is observed to increase over the duration of the time series, but it is unclear as to whether this is entirely a monotonic increase (periodic phase) or part of a rise-and-fall (quasi-periodic phase). If we are truly observing the periodic phase of the wave, then the observed group velocity is likely to be close to v_{Ae} than v_A. In this case, the local magnetic field is more likely to be ~ 25 G, a reasonable value for the coronal field.

As a final point of interest in this comparison, Berghmans et al. (1996) also find that contributions from behind the initial wavefront can leak to the loop's more tenuous exterior, and overtake the leading wavefront due to the higher external Alfvén velocity, v_{Ae}, returning to the loop to contribute a negative-amplitude (dark) disturbance ahead of the wave within the loop. If we examine more closely the intensity of the wave in Fig. 3, we see that there indeed appears to be such a darkening ahead of the leading bright edge in the fast-mode wave.

5 CONCLUSIONS

We present ground-based eclipse observations, taken on 1999 August 11, of a travelling wave in an active region coronal loop. The loop is characterized by an enhancement of density ($\rho_0/\rho_{ext} \approx 2.5$) with an estimated local magnetic field strength ~ 25 G. The wave is observed to travel with a velocity (perpendicular to the line-of-sight) an order of magnitude greater than the local sound speed. For this reason, we believe the wave to be an impulsively driven, fast-mode magneto-acoustic wave. It is not really possible to say whether the wave conforms to the periodic or quasi-periodic phases of an impulsively generated fast-mode wave, because of low signal-to-noise ratio in the Fe XIV channel with which we observed the wave. This is further compounded by the fact that the associated oscillation is only detected in the second half of our time series, which is limited to the first 40 s of the 1999 total solar eclipse. The wave does appear to fit aspects of the model of Berghmans et al. (1996) with respect to impulsively generated fast-mode waves, in particular the appearance of a darkening before the wave's leading maximum. In a follow-up article, it is our intention to more deeply investigate the observational signatures of the wave seen here, and to test their agreement with current models of quasi-periodic MHD disturbances. Using model parameters appropriate to our observations, we hope to determine whether the observed wave may in fact heat its host coronal loop.

REFERENCES

Berghmans D., De Bruyne P., Goossens M., 1996, ApJ, 472, 398
Brosius J. W., Davila J. M., Thomas R. J., Thompson W. T., 1994, ApJ, 425, 343

Dere K. P., Landi E., Mason H. E., Monsignori-Fossi B. C., Young P. R., 1997, A&AS, 125, 149

McKenzie D., Mullan D., 1997, Sol. Phys., 176, 127

Pasachoff J. M., Landman D. A., 1984, Sol. Phys., 90, 325

Phillips K. J. H. et al., 2000, Sol. Phys., 193, 259

Porter L. J., Klimchuk J. A., Sturrock P. A., 1994a, ApJ, 435, 482

Porter L. J., Klimchuk J. A., Sturrock P. A., 1994b, ApJ, 435, 502

Roberts B., Edwin P. M., Benz A. O., 1984, ApJ, 279, 857

Rudawy P., Rompolt B., Berlicki A., Buckylko L., Phillips K. J. H., Gallagher P. T., Williams D. R., Keenan, F. P., 2002, in Mishev D. N., Phillips K. J. H., eds, Proc. International Conf., First Results of the 1999 Total Eclipse Observations. Marin Drinov Academic Publishing House, Sofia, in press

Singh J. et al., 1997, Sol. Phys., 170, 235

Williams D. R. et al., 2001, MNRAS, 326, 428

Zhang J., White S. M., Kundu M. R., 1999, ApJ, 527, 977

This paper has been typeset from a T$_{\rm E}$X/L$^{\rm A}$T$_{\rm E}$X file prepared by the author.